

Gate-Voltage Control of Chemical Potential and Weak Antilocalization in Bi_2Se_3

J. Chen,¹ H. J. Qin,¹ F. Yang,¹ J. Liu,¹ T. Guan,¹ F. M. Qu,¹ G. H. Zhang,¹ J. R. Shi,² X. C. Xie,^{1,2} C. L. Yang,¹ K. H. Wu,^{1,*}
Y. Q. Li,^{1,†} and L. Lu¹

¹*Institute of Physics, Chinese Academy of Sciences, Beijing 100190, China*

²*International Center for Quantum Materials, Peking University, Beijing 100871, China*

(Received 7 March 2010; published 19 October 2010)

We report that Bi_2Se_3 thin films can be epitaxially grown on SrTiO_3 substrates, which allow for very large tunability in carrier density with a back gate. The observed low field magnetoconductivity due to weak antilocalization (WAL) has a very weak gate-voltage dependence unless the electron density is reduced to very low values. Such a transition in WAL is correlated with unusual changes in longitudinal and Hall resistivities. Our results suggest a much suppressed bulk conductivity at large negative gate voltages and a possible role of surface states in the WAL phenomena.

DOI: 10.1103/PhysRevLett.105.176602

PACS numbers: 72.15.Rn, 03.65.Vf, 71.70.Ej, 73.25.+i

A new state of matter, coined as topological insulator [1,2], was recently discovered to exist in 3D [3,4]. It is characterized by an insulating bulk and conducting surface states of massless helical Dirac fermions as a consequence of strong spin-orbit coupling [5–8]. The surface of the topological insulator can be viewed as a novel type of two-dimensional electron system that may be a fertile ground for exploring exciting new physics [2]. Among all known materials that could host the topological surface states [9–12], bismuth selenide (Bi_2Se_3) is most attractive because of a large band gap (~ 0.3 eV) in the bulk and a single Dirac cone in the surface energy spectrum, as confirmed in a photoemission experiment [10].

Despite numerous theoretical proposals that attempt to exploit their exotic properties, the 3D topological insulators have so far been confirmed to exist only in an ultrahigh vacuum (UHV) environment [4,10–15]. All of the previously reported transport studies have been bothered by a conducting bulk [16–19]. Even under circumstances of UHV, suppression of the bulk conductivity appears to be a challenging task. Tuning the chemical potential in Bi_2Se_3 was first realized with NO_2 molecules deposited onto the Bi_2Se_3 surface [20]. This method is, however, cumbersome, if not impossible, for preparing devices suitable for transport studies. Therefore, it is very important to find a more convenient means to lower the chemical potential in order to bring the surface states into the so-called topological transport regime.

According to theory, the Berry's phase associated with the helical surface states should result in weak antilocalization (WAL) in the electron transport [3]. In contrast with topologically trivial 2D systems with strong spin-orbit coupling [21], there will be no crossover from WAL to weak localization in a topological insulator as magnetic field increases. Detailed knowledge in the quantum corrections of magnetoconductivity may provide an alternative technique for identifying topological surface states, which has so far been limited to surface probing techniques.

Here we report that large tunability in the chemical potential in Bi_2Se_3 is achieved with a back gate. The gate-voltage dependencies of longitudinal and Hall resistivities as well as the WAL part of magnetoconductivity coherently point to a much depleted bulk and possible relevance of the surface states.

The Bi_2Se_3 films were grown on $\text{SrTiO}_3(111)$ substrates with molecular beam epitaxy. Figure 1(a) shows an *in situ* STM image of a Bi_2Se_3 thin film. It displays many triangular-shaped flat terraces with a step height close to 1 nm, corresponding to one quintuple-layer (QL). The QL-by-QL growth mode of Bi_2Se_3 [22] enabled us to precisely control the film thickness. A 50 nm thick Pd film was subsequently deposited onto the back of the substrate to serve as a back gate. In order to minimize

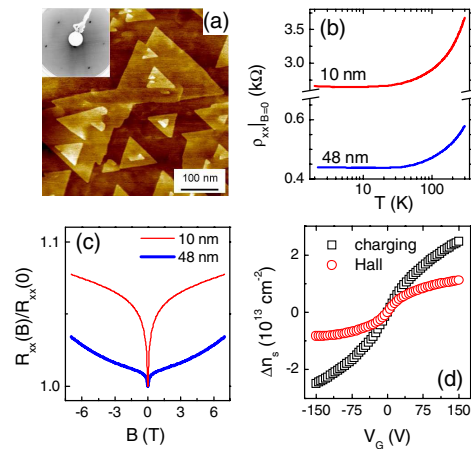


FIG. 1 (color online). (a) STM image and low energy electron diffraction pattern (inset) of a Bi_2Se_3 single crystalline thin film grown on a $\text{SrTiO}_3(111)$ substrate; (b) T dependence of ρ_{xx} of samples A (lower) and B (upper) at $B = 0$; (c) normalized magnetoresistance of samples A (lower) and B (upper); (d) relative changes in carrier density with respect to $V_G = 0$ extracted from Hall measurements (circles) and charging effects (squares).

the surface degrading effects at ambient conditions [23], we patterned the Bi_2Se_3 films into Hall bars of millimeter sizes with a fine diamond pen so that heating procedures in the standard lithography process were avoided.

The electron transport measurements were carried out in a cryostat with B up to 7 T and at temperature $T = 1.8$ K. Hall measurements showed that undoped Bi_2Se_3 films are of n type. Dozens of devices with various carrier densities and gating strengths have been measured. The data to be presented here were mainly recorded from two samples. Sample *A* is a 48 nm thick undoped Bi_2Se_3 film, whereas sample *B* is 10 nm thick and doped with calcium in order to lower the electron density [24]. Similar gating effect on weak antilocalization was also observed for undoped Bi_2Se_3 samples in which stronger gating strength (evidenced by for instance, reversal of the sign of the Hall resistivity) was achieved.

As shown in Fig. 1(b), the longitudinal resistivities at $B = 0$ (ρ_{xx}^0) of samples *A* and *B* have similar temperature dependence. When a perpendicular magnetic field is applied, both samples show positive magnetoresistance (MR) with a cusplike minimum at $B = 0$. The MR of sample *A* in large fields has a parabolic B dependence, which is not observed in sample *B*. The Hall resistivities (ρ_{xy}) of both samples varies linearly with B without any noticeable curvature. The electron densities extracted from the Hall coefficients are $n_s^{\text{Hall}} = -1/(eR_H) \approx 3.7$ and $1.1 \times 10^{13} \text{ cm}^{-2}$ for samples *A* and *B*, respectively.

The electron density can be modified substantially by applying the gate-voltage V_G . Figure 1(d) shows the relative changes in the carrier density in sample *B* with respect to n_s at $V_G = 0$. They were measured with a charging experiment, in which a constant current of 1 nA was used to charge the $\text{Bi}_2\text{Se}_3/\text{STO}/\text{Pd}$ capacitor. The recorded charging time during the change of V_G thus provided a measurement of the variation in the *total* charge density in the top electrode. It has a nonlinear dependence on V_G , which is a typical dielectric response of STO single crystals to the applied electric fields [25]. The relative change in the total carrier density with respect to n_s at $V_G = 0$, Δn_s , reaches $\pm 2.5 \times 10^{13} \text{ cm}^{-2}$ at $V_G = \pm 150$ V, demonstrating a superb capability in tuning n_s .

As shown in Fig. 1(d), the relative changes in n_s extracted from the Hall measurements, Δn_s^{Hall} , are significantly smaller in magnitude than Δn_s . This suggests that the Hall measurements give underestimated n_s values, even though ρ_{xy} has a linear dependence on B . This is not surprising because multiple types of charge carriers coexist in the Bi_2Se_3 film. According to the photoemission studies [10,13,19,20], the energy difference between the conduction band minimum and the Dirac point of the surface states is only about 0.2 eV. This means that the two surfaces in the topological regime can only hold up to about 0.5×10^{13} electrons/cm². Therefore, even in sample *B*, which has a very low density, there exist a large number of conduction band electrons at $V_G = 0$. Considering that

the bottom and top surfaces have different interfaces, we expect at least three different types of charge carries in the device, namely, the bulk electrons and the carriers related to the top and the bottom surface states.

Figure 2 shows the carrier density dependence of longitudinal resistivity ρ_{xx}^0 and n_s^{Hall} . When n_s is lowered, ρ_{xx}^0 increases monotonically, but its derivative, $d\rho_{xx}^0/dn_s$, has a minimum at $\Delta n_s \approx -1.9 \times 10^{13} \text{ cm}^{-2}$, where the slope of $d\rho_{xx}^0/dn_s$ changes its sign from positive to negative abruptly. Unusual features are also present in n_s^{Hall} . The derivative dn_s^{Hall}/dn_s does not vary smoothly with n_s . It also shows a sharp transition at about $-1.9 \times 10^{13} \text{ cm}^{-2}$.

Based on these observations, we divide the negative Δn_s region in Fig. 2 into three zones to represent different degrees of carrier depletion. In zone I, which spans from 0 to $-1.0 \times 10^{13} \text{ cm}^{-2}$, ρ_{xx}^0 varies very slowly. The magnitude of $d\rho_{xx}^0/dn_s$ increases rapidly in zone II ($-1.9 < \Delta n_s < -1.0 \times 10^{13} \text{ cm}^{-2}$). This is normally what one would expect from depleting a typical semiconductor layer. At sufficiently low densities, metal-insulator-transition may take place in the bulk and the rapid increase in $|d\rho_{xx}^0/dn_s|$ in zone II may be a precursor for such a transition. When $\Delta n_s < -1.9 \times 10^{13} \text{ cm}^{-2}$ (zone III), further depletion leads to the suppression of the bulk conductivity and hence the transport is dominated by the surface (or interface) states. This could account for the sudden change in the slope of $d\rho_{xx}^0/dn_s$. Another noteworthy feature in this deep depletion regime (zone III) is that n_s^{Hall} only varies from 0.31 to $0.24 \times 10^{13} \text{ cm}^{-2}$. Its slope becomes nearly zero when Δn_s approaches to the lower limit. This would be difficult to explain if every part of the sample still remained n type. A likely scenario is that the chemical potential at the bottom surface has dropped below the Dirac point.

The profile of the chemical potential for a given Δn_s can be calculated by solving the 1D Poisson equation. For the simplest case, we do not consider band bending near the bottom or top surfaces at $V_G = 0$. If we assume

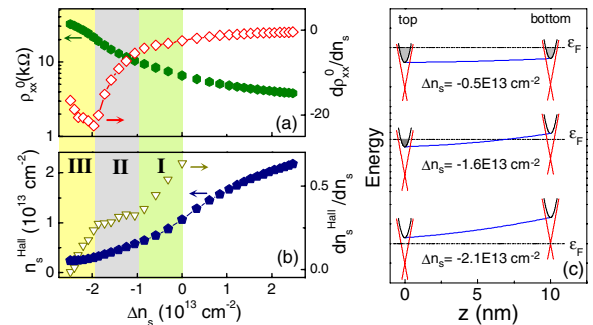


FIG. 2 (color online). Plotted as a function of Δn_s are (a) ρ_{xx}^0 (hexagons) and its derivative (diamonds); (b) n_s^{Hall} (pentagons) and its derivative (triangles). The negative gate voltages are partitioned into three zones (I, II, III) according to the degree of carrier depletion. (c) Calculated band diagrams based on a simple model described in the text.

a bulk electron density of $1 \times 10^{19} \text{ cm}^{-3}$, $\Delta n_s \approx -2 \times 10^{13} \text{ cm}^{-2}$ is then required to reach the situation in which the chemical potential on the top surface is lowered to the conduction band minimum. Figure 2(c) displays three band diagrams calculated for $\Delta n_s = -0.5, -1.6,$ and $-2.1 \times 10^{13} \text{ cm}^{-2}$, which may provide a crude picture for the evolution of the chemical potential and the carrier depletion as V_G decreases. Many experimental factors, for instance, the band bending and charge trapping effects near the top or bottom surfaces as well as impurity levels, can certainly modify the results quantitatively. Nevertheless, the basic trend shown in Fig. 2(c) should remain intact.

Figure 3 shows a detailed gate-voltage dependence of magnetoconductivity of samples A and B. It is defined as $\Delta\sigma(B) = \sigma_{xx}(B) - \sigma_{xx}|_{B=0}$. For both samples $\Delta\sigma(B)$ has a cusplike maximum at $B = 0$, which is typical for the weak antilocalization. For sample A [Fig. 3(a)], within the range of all accessible carrier densities, the low field part of $\Delta\sigma(B)$ varies very little.

The gate-voltage dependence of the magnetoconductivity of sample B is shown in Figs. 3(b) and 3(c). For positive gate-voltages, all $\Delta\sigma(B) - B$ curves are nearly identical, even though there are more than a factor of 2 change in R_H and an increase of $2.5 \times 10^{13} \text{ cm}^{-2}$ in n_s . In contrast, when V_G is lowered to -60 V and below, $\Delta\sigma(B)$ varies drastically with V_G . Measurements on several other samples with various carrier densities that spread between those of samples A and B further confirm the following observation: the back-gate voltage can induce a *significant* amount of change in the low field magnetoconductivity only when the carrier density is extremely low.

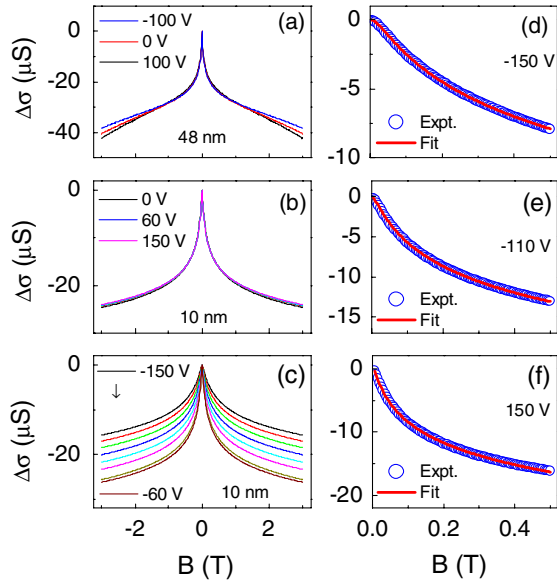


FIG. 3 (color online). Magnetoconductivity, defined as $\Delta\sigma(B) = \sigma_{xx}(B) - \sigma_{xx}|_{B=0}$ of (a) sample A; (b) sample B at $V_G = 0, 60,$ and 150 V ; (c) sample B at $V_G = -150 \text{ V}, -140, -130, -120, -110, -100, -80,$ and -60 V (from top to bottom). Fitted curves (lines) with Eq. (1) are also shown in (d) $V_G = -150 \text{ V}$, (e) -110 V , and (f) 150 V for sample B.

In case of coexistence of a bulk Fermi surface with the surface states, the Bi_2Se_3 thin films may be treated as traditional 2D electron systems with strong spin-orbit interaction. The Hikami-Larkin-Nagaoka (HLN) equation [26] is often applied to account for the magnetoconductivity in this type of systems. In the limit of very strong spin-orbit interaction and low mobility, i.e., $\tau_\phi \ll \tau_{so}$ and $\tau_\phi \ll \tau_e$, the HLN equation is reduced to

$$\Delta\sigma(B) \approx -\alpha \cdot \frac{e^2}{2\pi^2\hbar} \left[\psi\left(\frac{1}{2} + \frac{B_\phi}{B}\right) - \ln\left(\frac{B_\phi}{B}\right) \right], \quad (1)$$

where τ_{so} (τ_e) is the spin-orbit (elastic) scattering time, $\alpha = 1/2$, ψ is the digamma function, and $B_\phi = \hbar/(4De\tau_\phi)$ is a characteristic field related to the dephasing time τ_ϕ . Here D is the diffusion constant. For the surface states in the topological regime, to the best of our knowledge, no theory has yet been given to quantitatively describe the weak antilocalization arising from the Berry's phase of the Dirac fermions [3,14]. We notice, however, that McCann *et al.* [27] developed a theory for graphene, in which WAL could be suppressed by intervalley scatterings as well as chirality-breaking intravalley scatterings by lattice defects. These effects are absent in the single-cone spin-helical system encountered here, so we expect that the magnetoconductivity of *one* topological surface of Bi_2Se_3 follows the same form as Eq. (1) with $\alpha = 1/2$ [28]. As shown in Figs. 3(d)–3(f), Eq. (1) does provide reasonably good fits to the data at all gate voltages.

Figure 4(a) displays detailed fitting results for sample B. B_ϕ varies very little for a wide range of densities, i.e., $\Delta n_s = -1.4$ to $+2.5 \times 10^{13} \text{ cm}^{-2}$. When n_s becomes lower (in zone II), B_ϕ starts to vary appreciably with V_G . It is striking that B_ϕ nearly triples in a very narrow range of carrier densities in zone III. The correlation between the WAL data and ρ_{xx} is shown more clearly in the $B_\phi\sigma_{xx}^0 - \Delta n_s$ plot [Fig. 4(b)], which has a minimum at the boundary between zones II and III.

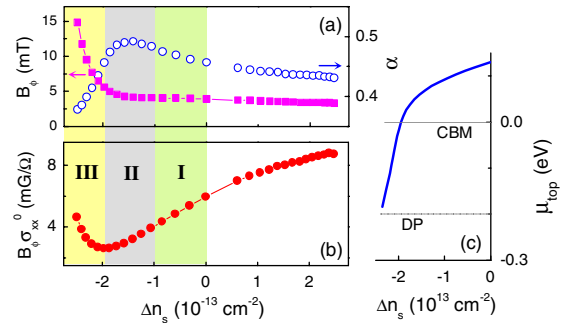


FIG. 4 (color online). (a) B_ϕ (solid squares) and α (open circles), (b) $B_\phi\sigma_{xx}^0$, as a function of Δn_s . Here σ_{xx}^0 is the conductivity at $B = 0$. The partition of the negative V_G region is the same as that in Fig. 2. (c) Calculated chemical potential on the top surface with respect to the conduction band minimum (CBM). The Dirac point (DP) is located at -0.2 eV .

The coefficient α extracted with Eq. (1) is close to $1/2$ for all carrier densities. One possible explanation is that the Bi_2Se_3 thin film can be treated as a 2D system described by the HLN equation, but it is difficult to reconcile with the fact that B_ϕ increases by less than 15% for a wide range of densities ($\Delta n_s = -1.4$ to $2.5 \times 10^{13} \text{ cm}^{-2}$), while ρ_{xx} and n_s^{Hall} are changed by a factor of 3.4 and 4.7, respectively. Such large changes are usually reflected in D and τ_ϕ , and B_ϕ would change accordingly.

An alternative explanation might come from treating the top and bottom surface states as well as the bulk electrons separately. Since both surfaces were measured simultaneously in the experiment, this would lead to $\alpha = 1$ if they contribute equally. Apparently this is not the case. Considering that V_G is applied from the back of the sample, the electron states at and near the bottom surface will be influenced before any large impact can be exerted on the top surface [see Fig. 2(c)]. The weak carrier density dependence of B_ϕ for such a wide range of V_G implies that the bottom surface or the nearby bulk does not contribute much to the magnetoconductivity at low fields. It rather mainly originates from the electron states at or near the top surface. This may be understood as follows. The bottom surface has many defects because of the lattice mismatch with the STO substrate. Because of the layered nature of the Bi_2Se_3 crystal and lattice relaxation during the growth, the top surface is expected to be of considerably better quality. Consequently, the top surface has much higher carrier mobility and thus smaller B_ϕ . This results in negligible contribution from the bottom surface. Furthermore, the Bi_2Se_3 crystal has inversion symmetry, which may account for insignificant contribution from the bulk.

If the low field magnetoconductivity is indeed mainly contributed by the states at or near the top surface, the large increase in B_ϕ in zone III can be explained qualitatively. In this low density regime, we anticipate a significant drop in the local chemical potential at the top surface as V_G becomes more negative [Fig. 4(c)]. For a 2D system the diffusion constant is $D = 1/2 v_F^2 \tau_e$, where the Fermi velocity v_F is constant for Dirac fermions. The larger B_ϕ at lower densities can therefore be attributed to reduced screening and stronger electron-electron interaction effects, which are known to shorten τ_e and τ_ϕ . In case the conduction band electrons are not fully depleted near the top surface, similar arguments can also be applied. The corresponding n_s dependence of B_ϕ should, however, be *qualitatively* different because the dimensionality of the electron system is changed from 2D to 3D (or quasi-2D). The $B_\phi \sigma_{xx}^0$ minimum observed near the boundary between zones II–III in Fig. 4(b) might be associated with a transition of the electron states from a bulklike to a more surface-dominating type.

Finally, we briefly remark on the coefficient α , which has a sizable, density-dependent deviation from $1/2$. This

is not expected from the theories mentioned above. Possible explanations may arise from electron-electron interaction effects [29], as well as defects in Bi_2Se_3 . Furthermore, the large electric field induced by the back-gate voltage might significantly modify the spin-orbit interaction via the Rashba effect [13,30]. A thorough explanation of the data is out of the scope of this Letter, but it certainly deserves further work.

We are grateful to D. Maryenko, K. Chang, Y.L. Chen, N. Cooper, X. Dai, Z. Fang, and K. He for stimulating discussions. We acknowledge financial support from Ministry of Science & Technology of China, NSF-China, and Chinese Academy of Sciences.

*khwu@iphy.ac.cn

†yqli@iphy.ac.cn

- [1] X.L. Qi and S.-C. Zhang, *Phys. Today* **63**, No. 1, 33 (2010).
- [2] M.Z. Hasan and C.L. Kane, arXiv:1002.3895 [Rev. Mod. Phys. (to be published)], and references therein.
- [3] L. Fu and C.L. Kane, *Phys. Rev. B* **76**, 045302 (2007).
- [4] D. Hsieh *et al.*, *Nature (London)* **452**, 970 (2008).
- [5] L. Fu, C.L. Kane, and E.J. Mele, *Phys. Rev. Lett.* **98**, 106803 (2007).
- [6] J.E. Moore and L. Balents, *Phys. Rev. B* **75**, 121306(R) (2007).
- [7] A.P. Schnyder *et al.*, *Phys. Rev. B* **78**, 195125 (2008).
- [8] X.L. Qi, T.L. Hughes, and S.-C. Zhang, *Phys. Rev. B* **78**, 195424 (2008).
- [9] H.J. Zhang *et al.*, *Nature Phys.* **5**, 438 (2009).
- [10] Y. Xia *et al.*, *Nature Phys.* **5**, 398 (2009).
- [11] Y.L. Chen *et al.*, *Science* **325**, 178 (2009).
- [12] D. Hsieh *et al.*, *Phys. Rev. Lett.* **103**, 146401 (2009).
- [13] Y. Zhang *et al.*, *Nature Phys.* **6**, 584 (2010).
- [14] P. Roushan *et al.*, *Nature (London)* **460**, 1106 (2009).
- [15] T. Zhang *et al.*, *Phys. Rev. Lett.* **103**, 266803 (2009).
- [16] A.A. Taskin and Y. Ando, *Phys. Rev. B* **80**, 085303 (2009).
- [17] J.G. Checkelsky *et al.*, *Phys. Rev. Lett.* **103**, 246601 (2009).
- [18] H. Peng *et al.*, *Nature Mater.* **9**, 225 (2010).
- [19] J.G. Analytis *et al.*, *Phys. Rev. B* **81**, 205407 (2010).
- [20] D. Hsieh *et al.*, *Nature (London)* **460**, 1101 (2009).
- [21] G. Bergmann, *Phys. Rep.* **107**, 1 (1984).
- [22] G.H. Zhang *et al.*, *Appl. Phys. Lett.* **95**, 053114 (2009).
- [23] J.G. Analytis *et al.*, arXiv:1003.1713.
- [24] Y.S. Hor *et al.*, *Phys. Rev. B* **79**, 195208 (2009).
- [25] H.-M. Christen *et al.*, *Phys. Rev. B* **49**, 12095 (1994).
- [26] S. Hikami, A.I. Larkin, and Y. Nagaoka, *Prog. Theor. Phys.* **63**, 707 (1980).
- [27] E. McCann *et al.*, *Phys. Rev. Lett.* **97**, 146805 (2006).
- [28] The coefficient α would be $4 \times 1/2 = 2$ for an infinite graphene sheet free of imperfections.
- [29] P.A. Lee and T.V. Ramakrishnan, *Rev. Mod. Phys.* **57**, 287 (1985).
- [30] W. Knap *et al.*, *Phys. Rev. B* **53**, 3912 (1996).